# BOULDER TRACKS AND NATURE OF LUNAR SOIL

H. JOHN HOVLAND and JAMES K. MITCHELL
*Geotechnical Engineering, University of California, Berkeley, Calif., U.S.A.*

(Received 7 September, 1972)

**Abstract.** Boulder tracks from 19 different locations on the Moon, observable in Lunar Orbiter photographs, have been examined. Measurements of the track width indicate that some of the boulders sank considerably deeper than others. It is suggested that lunar surface materials vary from place to place; the state of compaction (density of lunar soil) is probably one of the significant variables. Using bearing capacity theory, modified to be applicable to the rolling boulder problem by theoretical studies and extensive testing, the friction angle of the lunar soil was estimated. Most of the results were between 24 and 47 degrees with an arithmetic average of 37 degrees. These values suggest corresponding density variations of 1.25 to 2.00 g/cm$^3$.

## 1. Introduction

Among the conspicuous and interesting features on the lunar surface are large boulders and the tracks they left as they rolled down slopes. The tracks appear to have been caused by rolling, bouncing, and skidding. More than 300 such tracks have been identified in photography taken from lunar orbit (Grolier *et al.*, 1968). Examples of typical tracks formed by rolling and bouncing boulders are shown in Figure 1.

Since a relationship, which includes both soil and boulder geometry and properties, must exist between the size and the track of the boulder, a number of lunar boulders have been studied (Filice, 1967; Nordmeyer and Mason, 1967; Eggleston *et al.*, 1968; Moore, 1970; Moore *et al.*, 1972) in an effort to determine the static bearing capacity of lunar surface soil. Moore's analysis is the most comprehensive of

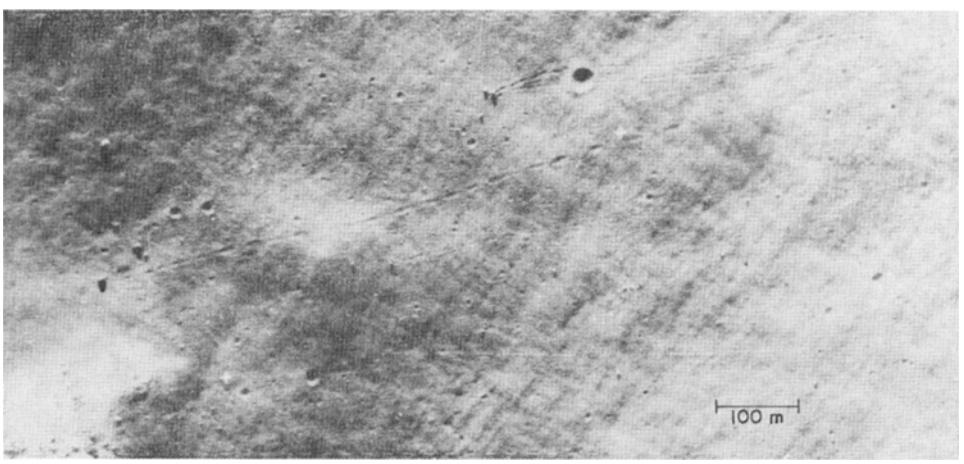


Fig. 1. Typical boulder tracks. (North rim of Gassendi, Lunar Orbiter V, Frame 179.)

*The Moon* **6** (1973) 164–175. 

those reported to date. From static analyses of 48 lunar blocks and boulders and their tracks he obtained friction angles (arctangent of the coefficient of friction) between 10° and 30° with an average of 17°. These values are considerably less than have been deduced from the Surveyor Program (Scott and Roberson, 1969) and from Apollo soil mechanics measurements (Mitchell *et al.*, 1971, 1972), where values generally greater than 35° have been obtained. We have investigated independently soil strength parameters and densities as indicated by lunar boulder tracks. Our investigations are based on extensive experimentation and a different theoretical concept, as described below.

## 2. Theory

A rolling boulder is illustrated in Figure 2a, and a boulder that has come to rest is illustrated in Figure 2b. While Moore determines the bearing pressure for a boulder that has come to rest, as the weight of the boulder divided by the total boulder-soil contact area, we determine the bearing pressure for a rolling boulder. The rolling phenomenon requires that only the front part of the boulder in the rut is in contact with the soil. If the boulder-soil contact area is to be determined from the measured

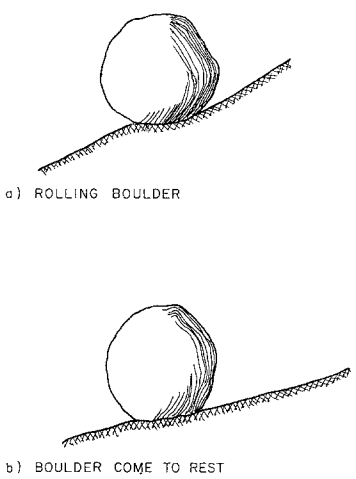


Fig. 2. Longitudinal section of boulder and track.

track width, the contact area for a spherical boulder would be approximately circular for a boulder that has come to rest, but semi-circular and only half as large for a rolling boulder.

It is important to recognize that the results of these two approaches are not really comparable. Moore's approach leads to a more realistic determination of the bearing pressure for a boulder at rest, since he analyzes the actual shape of the boulder – be it spherical or prismatic. To calculate soil parameters, the bearing pressure so determined can not, however, be equated to the bearing capacity, because the soil is not at shear (a state of limiting equilibrium) for a boulder that has come to rest. In fact, analysis

(Moore *et al.*, 1972) shows that the theoretical bearing capacity under a boulder that has come to rest is likely to be considerably higher than the bearing pressure.

The soil is obviously at shear for the case of a rolling boulder, and, to calculate soil parameter, the bearing pressure can be equated to theoretical bearing capacity. In this theoretical analysis, it has, however, been necessary to assume that the boulder is spherical. Limitations of this assumption and a general description of both terrestrial and lunar boulders are presented by Moore *et al.* (1972). While soil parameters determined from a single boulder track could be considerably in error, the average and range of soil parameters determined from an adequate number of carefully selected boulder tracks can be quite meaningful.

Bearing capacity theory (Terzaghi, 1943; Meyerhof, 1951) was modified by theoretical studies and experimentation (Hovland and Mitchell, 1970) for application to the rolling sphere phenomenon. (Some 200 spheres were rolled on Yuma sand to investigate static and dynamic effects.) Calculated friction angle values using the modified theory and experimentally determined (triaxial) friction angle values are compared in Figure 3. The comparisons were made both for all rolling spheres (Figure 3a), and for spheres rolling at constant velocity (Figure 3b). The central dot indicates the mean, and the vertical bar indicates the standard deviation. Based on the theory, charts were prepared (Figure 4) for relating the track width to diameter ratio, $w/D$, for lunar

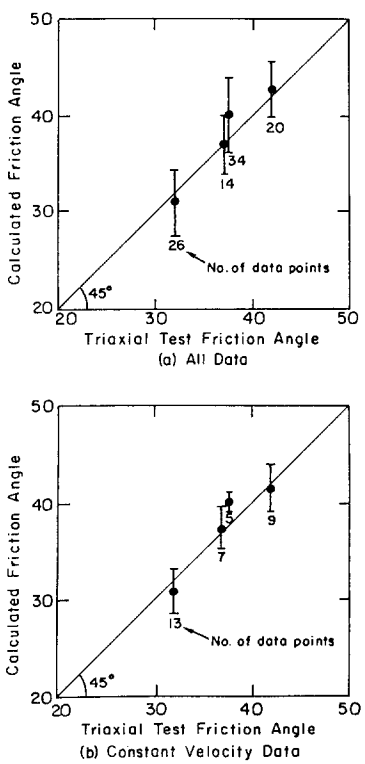


Fig. 3. Comparison between calculated and triaxial test friction angle values.

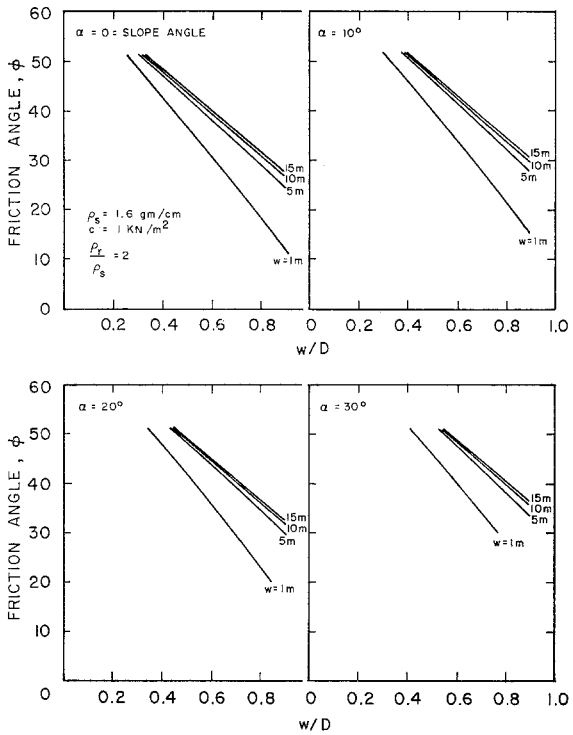


Fig. 4. Relationship between friction angle, $\phi$, and track width to sphere diameter ratio, $w/D$, for lunar soil.

boulder tracks to the friction angle, $\phi$, of lunar soil. In these charts, $\alpha$ = slope angle, $c$ = soil cohesion, $\varrho_s$ = soil density, and $\varrho_r$ = rock (boulder) density.

## 3. Lunar Boulder Tracks Selected for Study

Lunar Orbiter photography was carefully screened for suitable boulder tracks. Primarily we looked for relatively smooth and continuous tracks; such tracks are formed by relatively spherical, sub-rounded and equi-dimensional boulders. Sixty-nine boulder tracks from 19 locations on the Moon (Figure 5) were selected.

Most of the tracks appeared to originate on a relatively steep crater or rille slope. Three boulder tracks in Hadley rille seemed to originate at a layer of rock outcrop. Although the cause of rolling is not known in every case, possible conditions are:

(1) *Continuous phenomena*: Instability and rolling may be caused by general gravity-induced, downslope transportation of material, the build-up of fillets above a boulder, or the erosion of support under a boulder resting on a slope. Cyclic thermal expansion and contraction of rock and micrometeoroid impact may also loosen rock from its parent outcrop, shape a rounded boulder from an angular block, and cause rolling.

(2) *Erratic phenomena*: Some tracks have originated from blocks thrown out of

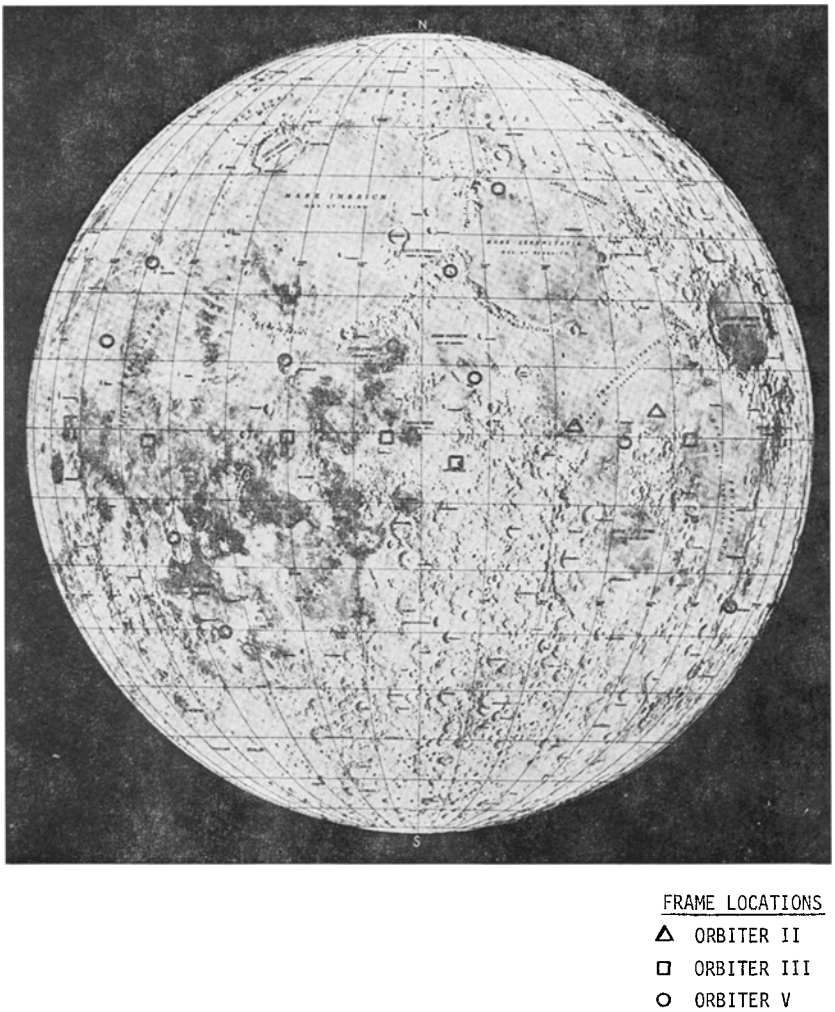


Fig. 5. Locations of boulder tracks analyzed.

impact craters. Seismic events (moonquakes) and impacts have undoubtedly also triggered the rolling of some boulders.

## 4. Analysis and Results

Track widths and boulder diameters for the 69 boulder tracks were measured from Orbiter photographs. These data were used in conjunction with the charts presented in Figure 4 to deduce the angle of internal friction for the soil at the different sites. Table I documents the location, track data, and calculated friction angle for each of the tracks studied. Figure 6a shows a frequency distribution of the measured trac-

Table I

| Location | Frame | Framelet (boulder location) | Longitude (degrees) | Latitude (degrees) | Boulder diam (D) (meters) | Track width (w) (meters) | Slope (α) (degrees) | $\frac{w}{D}$ | Φ (°) |
|---|---|---|---|---|---|---|---|---|---|
| Table 1a. Results of boulder track analysis, Orbiter II photographs | | | | | | | | | |
| Mare Tranquillitatis (Approx. 100 km from Apollo Site 1) | II-27H | 921 | 36.54 | 3.56 | 6.0 | 6.0 | 15 | 1.000 | 24 |
| Sabine D (Approx. 30 km from Surveyor 5 and Apollo Site 2) | II-76H | 364 | 23.68 | 1.20 | 8.7 | 6.4 | 13* | 0.736 | 36 |
| Sinus Medii (Approx. 20 km from Surveyor 6 and Apollo Site 3) | II-122H | 464 | -1.32 | 0.32 | 6.3 | 6.3 | 15 | 1.000 | 24 |
| Sinus Medii (Approx. 20 km from Surveyor 6 and Apollo Site 3) | II-123H | 594 + 15mm, 28 mm | -1.89 | 0.29 | 5.9 | 5.4 | 10 | 0.913 | 26.5 |
| * Slope angle primarily based on slope determined by photogrammetry. | | | | | | | | | |
| Table 1b. Results of boulder track analysis, Orbiter III photographs | | | | | | | | | |
| Mare Fecunditatis (Approx. 150 km WNW of Messier A) | III-35H | 396 + 4 mm, 258mm | 42.81 | -1.05 | 5.0 | 4.6 | 25 | 0.920 | 30.5 |
| N E Mösting | III-107H | 868 + 1mm, 21mm | -5.67 | -0.33 | 3.6 | 2.8 | 10 | 0.778 | 28 |
| Rima Hipparchus | III-111H | 364 + 1mm, 286mm | 4.83 | -4.92 | 5.2 | 5.2 | 30 | 1.000 | 28 |
| | | 373 + 13mm, 392mm | | | 6.0 | 4.9 | 10 | 0.816 | 31 |
| Reinhold (Approx. 30km E. of Reinhold K) | III-125H | 204 + 1.5mm, 69mm | -20.04 | -0.60 | 2.3 | 1.6 | 15 | 0.696 | 33 |
| | | 204 + 3mm, 75mm | | | 2.5 | 2.5 | 15 | 1.000 | 19 |
| | | 204 + 5mm, 76mm | | | 2.5 | 1.9 | 15 | 0.760 | 30 |
| | | 205 + 13mm, 53mm | | | 2.7 | 2.1 | 15 | 0.777 | 28.5 |
| | | 206 + 15mm, 64mm | | | 4.1 | 3.7 | 20 | 0.756 | 27 |
| Oceanus Procellarum (Approx. 40 km from Surveyor 1) | III-181H | 567 + 7mm, 284mm | -43.54 | -2.11 | 3.2 | 2.2 | 10 | 0.688 | 33 |
| Oceanus Procellarum (Approx. 40 km from Surveyor 1) | III-189H | 615 + 1mm, 77mm | -44.17 | -2.41 | 2.9 | 2.4 | 5 | 0.827 | 24 |
| | | 617 + 7mm, 91mm | | | 6.2 | 5.1 | 5 | 0.823 | 29.5 |
| Table 1c. Results of boulder track analysis, Orbiter V photographs. | | | | | | | | | |
| Central mountains of Petavius (rille) | V-34H | 880 + 12mm, 176mm | 60.57 | -25.70 | 23.3 | 13.7 | 20 | 0.586 | 45 |
| | | 891 + 6mm, 146mm | | | 19.0 | 13.7 | 20 | 0.720 | 40 |
| Mare Tranquillitatis (Approx. 40 km west of Censorinus) | V-63H | 738 + 14mm, 147mm | 32.75 | -0.44 | 7.35 | 4.8 | 0 | 0.653 | 36 |
| | | 738 + 16mm, 147mm | | | 8.2 | 6.0 | 0 | 0.731 | 33 |
| Large hill south of Alexander | V-88H** | 011 + 8.5mm, 230mm | 13.54 | 38.92 | 19.5 | 10.6 | 20 | 0.543 | 47 |
| S. E. part of Hyginus | V-95H* | 942 + 18mm, 365mm | 5.94 | 7.56 | 13.1 | 8.8 | 30 | 0.670 | 45 |
| | | 957 + 11.5mm, 164mm | | | 8.9 | 6.2 | 15 | 0.696 | 38 |
| | | 959 + 12.5mm, 161mm | | | 9.5 | 5.6 | 15 | 0.590 | 43 |
| | | 962 + 3mm, 167mm | | | 8.6 | 4.6 | 15 | 0.535 | 45 |
| | | 965 + 11mm, 239mm | | | 10.0 | 5.7 | 15 | 0.570 | 44 |
| | | 968 + 13mm, 253mm | | | 11.2 | 4.2 | 20 | 0.375 | 53.5 |
| | | 970 + 7mm, 246mm | | | 14.4 | 9.2 | 20 | 0.640 | 43 |
| | | 978 + 13mm, 252mm | | | 6.0 | 4.8 | 15 | 0.800 | 33 |
| | | 960 + 9mm, 146mm | | | 4.9 | 4.9 | 30 | 1.000 | 28 |

* Slope angle primarily based on slope determined by photogrammetry.
** Photogrammetrically determined slope is about 30°; 20° slope is primarily based on shadow technique.

Table I continued

| Location | Frame | Framelet (boulder location) | Longitude (degrees) | Latitude (degrees) | Boulder diam. (D) (meters) | Track width (w) (meters) | Slope (α) (degrees) | $\frac{w}{D}$ | $\phi$ (°) |
|---|---|---|---|---|---|---|---|---|---|
| Table Ic (Cont.) | | | | | | | | | |
| N E part of Hyginus | V-96H* | 092 + 1mm, 46mm | 5.96 | 7.85 | 15.9 | 10.6 | 10 | 0.666 | 39 |
| N E part of Hyginus | V-97H | 175 + 11mm, 268mm | 5.98 | 8.14 | 11.0 | 5.7 | 15 | 0.518 | 46 |
| | | 175 + 13mm, 275mm | | | 7.6 | 4.3 | 25 | 0.566 | 47 |
| | | 178 + 10mm, 224mm | | | 7.1 | 4.3 | 10 | 0.606 | 40 |
| | | 178 + 14mm, 222mm | | | 7.1 | 4.0 | 10 | 0.564 | 42 |
| | | 180 + 5mm, 230mm | | | 6.2 | 4.3 | 15 | 0.693 | 37.5 |
| | | 180 + 4mm, 229mm | | | 7.6 | 4.8 | 15 | 0.630 | 41 |
| | | 180 + 1mm, 235mm | | | 7.1 | 5.2 | 15 | 0.732 | 36 |
| Hadley Rille | V-105H* | 233 + 8mm, 232mm | 2.95 | 25.00 | 14.9 | 9.6 | 25 | 0.644 | 44.5 |
| | | 233 + 11mm, 234mm | | | 13.5 | 8.9 | 15 | 0.660 | 40 |
| | | 234 + 8mm, 235mm | | | 13.2 | 8.6 | 5 | 0.650 | 38 |
| Rima Bode | V-122H | 475 + 9mm, 121mm | -3.97 | 12.92 | 12.2 | 9.0 | 15 | 0.738 | 37 |
| Copernicus (center) | V-151H | 280 + 17mm, 184mm | -20.34 | 9.42 | 9.1 | 6.6 | 10 | 0.725 | 35.5 |
| | | 315 + 11mm, 282mm | | | 12.2 | 5.5 | 5 | 0.450 | 46.5 |
| Copernicus (NW of center) | V-155H | 845 + 14mm, 340mm | -20.24 | 10.58 | 10.6 | 4.8 | 0 | 0.452 | 45 |
| Copernicus (NW of center) | V-156H | 962 + 8mm, 135mm | -20.21 | 10.87 | 11.9 | 10.7 | 10 | 0.900 | 29 |
| Center of Vitello | V-168H | 518 + 9mm, 188mm | -37.57 | -30.61 | 19.2 | 19.2 | 15 | 1.000 | 27.5 |
| | | 519 + 1mm, 185mm | | | 11.4 | 5.4 | 10 | 0.474 | 46.5 |
| | | 520 + 2mm, 184mm | | | 8.0 | 4.8 | 15 | 0.600 | 42 |
| | | 520 + 9mm, 188mm | | | 11.9 | 7.9 | 15 | 0.664 | 40 |
| North rim of Gassendi | V-179H | 972 + 7mm, 250mm | -39.97 | -16.29 | 8.6 | 5.5 | 15 | 0.640 | 41 |
| | | 972 + 15mm, 333.4mm | | | 5.6 | 5.3 | 15 | 0.946 | 26 |
| | | 972 + 15.2mm, 338mm | | | 5.4 | 4.7 | 15 | 0.870 | 29.5 |
| | | 005 + 15mm, 244mm | | | 16.4 | 14.1 | 15 | 0.860 | 33 |
| | | 973 + 10mm, 345mm | | | 9.4 | 6.0 | 10 | 0.638 | 39.5 |
| | | 973 + 3mm, 285mm | | | 6.8 | 6.0 | 20 | 0.882 | 31.5 |
| | | 977 + 10mm, 340mm | | | 16.0 | 14.0 | 15 | 0.875 | 31 |
| | | 977 + 17mm, 325mm | | | 7.0 | 6.1 | 20 | 0.871 | 32 |
| | | 977 + 17mm, 305mm | | | 5.6 | 5.0 | 25 | 0.891 | 32 |
| | | 979 + 6mm, 352mm | | | 7.5 | 4.8 | 10 | 0.640 | 39 |
| Schröter's Valley | V-203H | 111 + 7mm, 246mm | 49.51 | 25.13 | 7.4 | 5.4 | 10 | 0.730 | 35 |
| | | 111 + 7mm, 246mm | | | 7.4 | 5.4 | 20 | 0.730 | 38 |
| Schröter's Valley | V-203H* | 227 + 8mm, 41mm | -49.48 | 25.52 | 9.4 | 6.2 | 15 | 0.660 | 40 |
| | | 221 + 18mm, 161mm | | | 12.6 | 6.5 | 5 | 0.516 | 44 |
| | | 210 + 15mm, 242mm | | | 12.6 | 7.2 | 15 | 0.572 | 44.5 |
| | | 210 + 14mm, 177mm | | | 10.5 | 5.5 | 25 | 0.524 | 49 |
| | | 202 + 7mm, 253mm | | | 19.4 | 12.3 | 20 | 0.634 | 43 |
| Oceanus Procellarum (Approx. 130 km NW of Marius) | V-213H | 417 + 7mm, 294mm | -56.03 | 13.50 | 7.4 | 4.3 | 20 | 0.580 | 44.5 |
| | | 431 + 10mm, 290mm | | | 6.4 | 3.3 | 15 | 0.515 | 44 |

width to boulder diameter ratio, $w/D$. Figure 6b shows a frequency distribution of the computed friction angle, $\phi$, values.

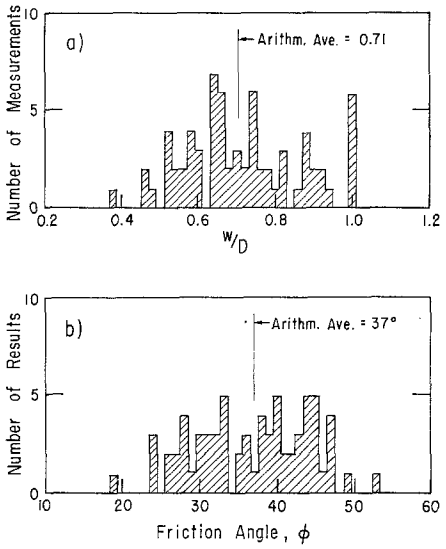


Fig. 6. Frequency distributions of measured $w/D$ and calculated friction angle.

## 5. Discussion

Since the track width to diameter ratio varied considerably for the boulder tracks investigated, some of the boulders sank considerably deeper than others. This implies a variability in soil properties which is reflected by the resulting friction angles, Figure 6b. It may be seen that $\phi$ ranged from 19° to 53°, with an arithmetic avarage of 37°. Most of the values of $\phi$ were between 24° and 47°. For this latter range, studies on simulated lunar soil (Houston *et al.*, 1970) indicate a density range of 1.25 to 2.00 g/cm$^3$. Analysis of data from near the ALSEP site on Apollo 15 (Mitchell *et al.*, 1972) yielded the following values: $\phi \simeq 45$–$50°$, $c = 1$ $kN/m^2$, $\varrho_s = 1.97$ g/cm$^3$. Thus the values deduced from the boulder tracks seem in reasonable accord with these values.

Certain slopes contained several boulder tracks. Data for these slopes are compared in Table II below. Data from all 19 locations are also averaged. The range of $w/D$ for any one location suggests local variability. The difference in the average $w/D$ from one location to another suggests regional variability; i.e., soil in the Reinhold location is probably weaker then soil in the Hyginus location. Footprint analysis (Houston *et al.*, 1972) suggest that at least for level intercrater areas, local variability may be more important than regional variability. (The footprint analyses lead to almost the same average density of 1.75 gm/cc for level intercrater areas for each of the Apollo 11, 12, 14, and 15 sites.)

The values of $\phi$ were also plotted against the boulder diameter as shown in Figure 7.

TABLE II

Comparison of data from slopes with several boulder tracks

| Location | Frame | Number of observations | Range of $w/D$ | Average $w/D$ | Range of $\phi°$ | Average $\phi°$ |
|---|---|---|---|---|---|---|
| Appr. 30 km E of Reinhold K | III–125H | 5 | 0.70–1.00 | 0.80 | 19–33 | 28 |
| SE part of Hyginus | V–95H | 9 | 0.38–1.00 | 0.65 | 28–53 | 41 |
| NE part of Hyginus | V–97H | 7 | 0.52–0.69 | 0.62 | 36–47 | 41 |
| North rim of Gassendi | V–179H | 10 | 0.64–0.95 | 0.81 | 26–41 | 34 |
| Schröter's valley | V–203H | 7 | 0.52–0.73 | 0.62 | 35–49 | 42 |
| All data | | 69 | 0.38–1.00 | 0.71 | 19–53 | 37 |

This figure suggests that for a given $w/D$ ratio the higher values of $\phi$ were associated with the larger boulders. This seems to imply the following:

(1) The friction angle for the lunar regolith increases with depth. This is probably a consequence of an increase in soil density with depth. Analogous behavior has been predicted from Apollo 15 soil mechanics experiments (Mitchell *et al.*, 1972).

(2) Alternatively, it is possible that the larger boulders were influenced by a layer of harder material below the lunar regolith. This could have resulted in a lower value of $w/D$ and an apparent high $\phi$ for the overlying soil. In this case the implication is that the thickness of the lunar regolith in the vicinity of the boulder tracks was close to the radius of the larger boulders (10 to 15 m).

The results of this study indicate a relatively large range for soil parameters ($19° < \phi < 53°$). It is appropriate, however, to assess the degree of confidence that may be placed in these results.

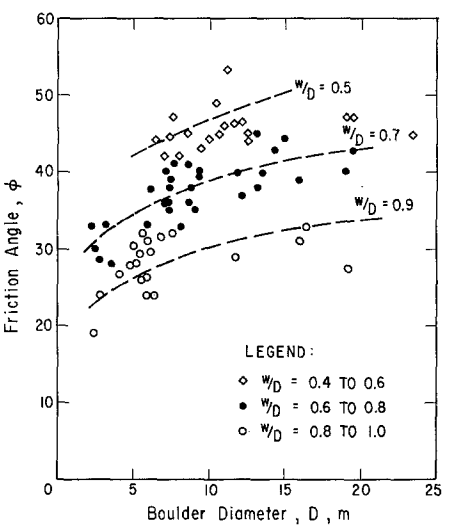


Fig. 7. Results of $\phi$ plotted against boulder diameter.

In developing the graphs shown in Figure 4, it was assumed that the lunar soil has a cohesion (c) of 1.0 $kN/m^2$, a density ($\varrho_s$) of 1.6 gm/cc, and a ratio of boulder density to soil density ($\varrho_r/\varrho_s$) of 2. As evidenced by Apollo sample data, these values for $\varrho_s$ and $\varrho_r/\varrho_s$ are reasonable averages for soil near the surface and lunar rocks. A cohesion of 1.0 $kN/m^2$ is near the upper bound for lunar soil studied directly thus far (Apollo 15).

What if these assumptions for lunar soil and rock properties were inappropriate, and estimates of the slope angle and boulder and track dimensions were wrong? To study the effect of these factors, theoretical determinations were made in turn for each variable of interest. Since many of the boulder tracks were close to the limit of resolution of the Orbiter photography, particular attention was given to the error introduced in measuring boulder and track dimensions. Measurements were, therefore, made on two different scale photographs. Differences in the two measurements were computed as follows:

For the diameter,

$$\Delta D = \left[1 - \frac{D_{\text{smaller}}}{D_{\text{larger}}}\right] \times 100.$$

For the track width,

$$\Delta w = \left[1 - \frac{w_{\text{smaller}}}{w_{\text{larger}}}\right] \times 100.$$

Similarly, the difference in the $w/D$ ratio was computed from

$$\Delta\left(\frac{w}{D}\right) = \left[1 - \frac{(w/D)_{\text{smaller}}}{(w/D)_{\text{larger}}}\right] \times 100.$$

The results of the comparison and the resulting change in the friction angle, $\Delta\phi$, are shown in Table III. (The basis for this comparison is $(w/D)_{\text{ave}} = 0.69$ and $\phi_{\text{ave}} = 37°$.)

TABLE III

Sensitivity of results to measurements.

| Comparison | $\Delta$D | $\Delta w$ | $\Delta\, w/D$ | $\Delta\phi$ |
|---|---|---|---|---|
| | (%) | (%) | (%) | (°) |
| Average | 9 | 12 | 9.6 | 2 |
| Maximum | 32 | 28 | 22 | 5 |

As shown in Table III above, the average difference in $\phi$ for the two measurements was about 2 degrees. If it can be assumed that the friction angle resulting from averaging the measurements, as was done for the results presented (Table I), is closer to the correct value than the result of either of the measurements independently, the friction angles presented in Table I may be regarded as including a one degree average error and about 3 degrees maximum error due to inconsistencies in measurements.

From a consideration of the possible effects of incorrect assumptions as to soil parameters, incorrect measurements, and incorrect estimates of the slope angle, probable uncertainties in the results can be summarized as follows:

| *Cause:* | *Effect on* $\phi(^\circ)$ |
|---|---|
| Variation in density ratio from $\varrho_r/\varrho_s = 1$ to 3 | $\pm 5$ |
| Variation in $c$ (for every $1 \times 10^4$ dyn/cm$^2$ change in $c$, for $c$ in the range of $10^3 \leqslant c \leqslant 10^5$ dyn/cm$^2$) | $\pm 1$ to 2 |
| Incorrect value of $w/D$ ratio (measurements) | $\pm 1$ to 2 |
| Incorrect slope angle ($\pm 5^\circ$) | $\pm 1$ to 2 |

Of the causes listed above, incorrect estimates of the density ratio have the largest effect on the results.

## 6. Conclusions

Provided that assumptions regarding other soil and rock parameters are realistic and that measurements of boulder and track dimensions are adequate, the analysis presented (Figure 4) makes it possible to estimate friction angle values for lunar and other extraterrestrial soils.

Measurements clearly indicate that some of the boulders left a considerably larger $w/D$ ratio than others. Possible implications of these variations are:

(1) The state of compaction of lunar soil may vary.
(2) The cohesion may vary.
(3) The friction angle may vary.
(4) The boulder density may vary.
(5) Differing ($w/D$) ratios may reflect differing ages of track.

Of the above, it is believed that the state of compaction of the lunar soil is one of the significant variables.

## Acknowledgements

This research was supported by National Aeronautics and Space Administration Contract NAS 8–21432, 'Lunar Surface Engineering Properties Experiment Definition' for Marshall Space Flight Center, Huntsville, Alabama.

## References

Eggleston, J. M., Patteson, A. W., Throop, J. E., Arant, W. H., and Spooner, D. L.: 1968, *Photographic Engineering* **34**, No. 3.

Filice, A. L.: 1967, *Science* **156**, 1486.

Grolier, M. J., Moore, H. J., and Martin, G. L.: 1968, Lunar Block Tracks, in *A Preliminary Geologic Evaluation of Areas, Photographed by Lunar-Orbiter V Including an Apollo Landing Analysis of One of the Areas*, U.S. NASA, Langley Research Center, Langley Working Paper (LWP) 506, pp. 143–154.

Hovland, H. J. and Mitchell, J. K.: 1970, *Mechanics of Rolling Sphere-Soil Slope Interaction*, Final Report, Vol. II of IV, Space Sciences Lab., NASA Contract NAS 8-21432, Univ. of Calif., Berkeley.

Houston, W. N., Namiq, L. I., and Mitchell, J. K.: 1970, *Lunar Soil Simulation*, Final Report, Vol. I of IV, Space Sciences Lab., NASA Contract NAS 8-21432, Univ. of Calif., Berkeley.

Houston, W. N., Hovland, H. J., Mitchell, J. K., and Namiq, L. I.: 1972, 'Lunar Soil Porosity and Its Variation as Estimated from Footprints and Boulder Tracks', *Proceedings 3rd Lunar Science Conf.*

Meyerhof, G. G.: 1951, *Geotechnique* II, 301.

Mitchell, J. K., Bromwell, L. G., Carrier, W. D., III, Costes, N. C., and Scott, R. F.: 1971, *Soil Mechanics Experiment*, in Apollo 14, Preliminary Science Report, NASA Spec. Publ., NASA SP-272, pp. 87-108.

Mitchell, J. K., Bromwell, L. G., Carrier, W. D., III, Costes, N. C., Houston, W. N., and Scott, R. F.: 1972, *Preliminary Analysis of Soil Behavior*, in Apollo 15, Preliminary Science Report, NASA Spec. Publ., NASA SP-289, pp. 7–1 to 7–28.

Moore, H. J.: 1970, *Estimates of Mechanical Properties of Lunar Surface Using Tracks and Secondary Impact Craters Produced by Blocks and Boulders*, USGS, Interagency Report, Astrogeology 22 (Preliminary).

Moore, H. J., Vischer, W. A., and Martin, G. L.: 1972, *Boulder Tracks on the Moon and Earth*, USGS, Prof. Paper 800-B. pp. B165–174.

Nordmeyer, E. F. and Mason, C. C.: 1967, *Lunar Surface Mechanical Properties Derived from Track Left by Nine Meter Boulder*, NASA, MSC Internal Note No. 67-TH-1.

Scott, R. F. and Roberson, F. I.: 1969, *Soil Mechanics Surface Sampler*, in Surveyor Program Results, NASA Spec. Publ., NASA SP-184, p. 171–179.

Terzaghi, K.: 1943, *Theoretical Soil Mechanics*, John Wiley and Sons, Inc., New York, 14th printing.